

Laser-combined STM for probing ultrafast transient dynamics

Yasuhiko Terada, Shoji Yoshida, Osamu Takeuchi and Hidemi Shigekawa

Institute of Applied Physics, CREST-JST, University of Tsukuba, Tsukuba 307-8573 Japan

<http://dora.bk.tsukuba.ac.jp>

Abstract

The development of time-resolved scanning tunnelling microscopy (STM), in particular, attempts to combine STM with ultrafast laser technology, is reviewed with emphasis on observed physical quantities and spatiotemporal resolution. Ultrashort optical pulse technology has allowed us to observe transient phenomena in the femtosecond range, which, however, has the drawback of a relatively low spatial resolution due to the electromagnetic wavelength used. In contrast, STM and its related techniques, although the time resolution is limited by the circuit bandwidth (~ 100 kHz), enable us to observe structures at the atomic level in real space. Our purpose has been to combine these two techniques to achieve a new technology that satisfies the requirements for exploring the ultrafast transient dynamics of the local quantum functions in organized small structures, which will advance the pursuit of future nanoscale scientific research in terms of the ultimate temporal and spatial resolutions.

PACS code: 07.79.Cz

1. Introduction

Making smaller and faster functional objects is a key factor for the development of nanoscale science and technology. The size of semiconductor devices, for example, decreases down to the nanoscale range. The device operation is currently dominated by atomic-scale properties, such as dopant distribution and surface/interface fluctuation, and thus is controlled by atomic-scale fabrication technology [1]. Accordingly, the operation speed exceeds GHz, and the understanding of carrier dynamics on an ultrashort timescale from the picosecond to nanosecond range is required. Therefore, developing devices with novel functions cannot be achieved without accurate evaluation of carrier dynamics under operation, in conjunction with exploring device physics. This has led to an increasing demand for a microscopic technique that allows the investigation of carrier dynamics at high spatial and temporal resolutions, in accordance with the surrounding potential, for example, modulated by atomic defects, dopant atoms, and local structures.

In conventional methods of measurement, one cannot use a detector to observe an ultrafast dynamic process occurring at a frequency exceeding its electrical bandwidth. In the field of ultrafast laser technology, there are numerous time-resolved optical spectroscopy methods that circumvent the problem of the bandwidth limit. The optical pump-probe technique is a representative example (figure 1), which has been reviewed by many groups [2, 3]. In the pump-probe technique, a sequence of paired laser pulses illuminates a sample. First (pump) pulses are used to excite the sample. After a certain delay time, the same area of the sample is illuminated by second (probe) pulses, and an optical response to probe pulses, such as reflectivity, transmissivity, and scattering light, is measured as a function of delay time. These optical properties depend on the excited state of the sample, and therefore, the time evolution of these quantities gives a measure of the relaxation process of the excited state. One only has to

measure a DC component, and the detector needs neither to be operated fast nor to have a wide bandwidth. The time resolution of the pump-probe technique is determined only by the optical pulse width and thus can be improved up to the femtosecond range. Other time-resolved techniques include the streak camera, optical Kerr gate, and up-conversion. An example of their recent applications is the analysis of time-resolved photoluminescence from a sample optically excited by an ultrashort pulse [4]. On the basis of these ultrafast optical techniques, various time-resolved microscopy methods have been developed.

Despite the ultrahigh temporal resolution achieved, the spatial resolution of real-space imaging using these optical techniques is determined by the diffraction limitation, and in general, it cannot be high. Several attempts have been made to overcome this limitation and achieve a high spatial resolution. The first example of such attempts is a combination of ultrafast laser technology with scanning near-field optical microscopy (SNOM). Examples of its recent applications are the analyses of spin-dependent photoluminescence using luminescence intensity correlation (with resolutions of 130 fs, 125 nm) [5], photoluminescence of a polymer blend using time-correlated single-photon counting (60 ps, 70 nm) [6], and pump-probe transmittance revealing carrier dynamics (250 fs, 150 nm) [7].

The second example of such attempts is the use of photoelectron emission microscopy (PEEM) to overcome the diffraction limit due to the photoemitted electrons, resulting in a high spatial resolution. Indeed, by combining time-resolved two photon photoemission with PEEM, Schmidt *et al* [8] firstly demonstrated the spatial resolution of about 20 nm. The same approach was used by several other research groups [9-14].

The third example is the use of ultrafast electron microscopy (UEM) that utilizes an ultrashort electron pulse, instead of an optical pulse, as a probe. The emerging area of UEM has been reviewed by King *et al* [15]. An optical pump pulse is used to excite a sample. Then, a

delayed optical pulse illuminates a photoactivated electron source to generate a probe electron pulse, and transmission images are stroboscopically recorded at a sequence of delay times. The following are the two types of ultrafast electron microscopes: a single-electron pulsed mode, developed by Zewail [16], is used for imaging reversible processes and records images stroboscopically. The other type, developed initially by Bostanjoglo [17] and subsequently by others [18, 19], is suitable for irreversible processes and records images in a single shot mode. UEM provides opportunities for studying dynamical changes in structural and morphological features (such as dislocations, impurity particles, grain boundaries, and phase boundaries) with a high spatiotemporal resolution both in real and reciprocal spaces, in many fields from material science to biology. The resolution of UEM depends on microscopic setups and has been discussed in detail by Gahlmann *et al* [20]. In the single-electron pulsed mode, each electron pulse, which has only one electron on average, eliminates the space charge effect and enables us to obtain a spatial resolution equivalent to that of conventional TEM. The temporal resolution is determined by the spread in the initial kinetic energy of the photoelectrons and the strength of the acceleration field. In the single-shot mode, in which high electron beam currents must be used, both the spatial and temporal resolutions are degraded by the electron-electron scattering effects due to Coulomb repulsion (space charge effect), which occurs when the electrons come closer to each other both before and after scattering by the specimen.

As described above, there have been numerous excellent time-resolved microscopic techniques achieving a high spatiotemporal resolution, with a wide field of application. However, it is still a challenge to attain an atomic-scale resolution in real-space imaging of ultrafast phenomena. Time-resolved scanning tunnelling microscopy (STM) is a promising candidate, because the tunnelling junction itself responds on a time scale of a few femtoseconds and principally ultrafast dynamics can be studied by STM. However, the

measurement bandwidth of an STM preamplifier is typically 100 kHz and 10 MHz at best [21-25], and faster dynamics is unavailable by standard STM.

We have aimed at developing a new microscopic technique with a high spatiotemporal resolution, by combining STM with ultrafast laser technology. In principle, a newly developed microscopic technique, shaken-pulse-pair-excited STM (SPPX-STM) [26-32] inherits the resolution of STM and the femtosecond resolution of the ultrashort pulse laser. By exciting a tunnelling junction between an STM tip and a sample by a sequence of paired pulses, and by detecting tunnelling current that depends on delay time between the pulses in a pair, one can analyze the time evolution of carrier density in a localized (nanoscale) region at subpicosecond ranges.

In this article, we briefly review attempts to improve resolutions by combining STM with ultrafast laser technology and describe the features and critical issues. Furthermore, we show the development of SPPX-STM and its principle and application.

2. Development of laser-combined STM for high time resolution

In analogy with optical pump-probe techniques, the limitation due to the circuit bandwidth is circumvented by the use of paired pulses. Since the invention of STM [33], many researchers have attempted to realize a high temporal resolution together with the atomic resolution of STM by combining STM with the pump-probe technique, but they mostly have succeeded only in revealing the difficulties in achieving the STM spatial resolution [34]. Some problems and limitations in pioneering time-resolved STM, photoconductively gated STM (PG-STM) and pulse-excited STM, and also the further development of SPPX-STM are discussed in this section.

2.1 Photoconductively gated STM (PG-STM)

A concept based on a fast photoconductive gate switch inserted into a detector circuit of STM current was realized and developed by several groups [35-37]. The scheme is called photoconductively gated STM (PG-STM). As in optical pump-probe techniques, a sequence of paired optical pulses is used. A pump pulse is used to excite a sample, and then, a probe pulse is used to illuminate a photoconductive gate to switch on the detector circuit (figure 2(b)). Thereby, the tunnelling current is gated and the ultrafast process is stroboscopically measured. This concept was mostly tested for detecting short voltage pulses propagating along a transmission line fabricated on a substrate, and the highest temporal resolution achieved thus far is around 1 ps [37]. In PG-STM, however, it was revealed that the detected signal originated from the geometric capacitance between the tip and the sample [38]. The signal measured by PG-STM is given by the averaged current of

$$I_c = \frac{1}{T} \int_0^T g_s(t')V(t')dt',$$

which integrates the periodic current pulses (T : repetition time of the ultrashort pulse laser) from the tip to form a quasi-dc current. Here, $V(t)$ is the time-dependent voltage that develops on the tip wire due to the short voltage pulses propagating along a transmission line, and $g_s(t)$ is a time-dependent conductance at the detection gap. Due to the existence of $g_s(t)$ associated with the detection gate switch, the measured signal I_c originates from the coupling between the tip wire and the stripline induced by the geometric capacitance. The tip capacitance has a spatial extent of the order of 10 μm , and hence, the spatial resolution of PG-STM also remains on the same order, incapable of detecting atomic-scale deviation in a time-dependent voltage process, such as a transient photovoltage process. As Groeneveld *et al* pointed out [38], one may still expect a high resolution for detecting laser-generated picosecond acoustic waves that lead to a time-dependent current, but an experimental demonstration has not yet been reported.

Another approach based on PG-STM has been made by the combination with the junction mixing technique [39-41]. As shown in figure 2(c), optical pump and probe pulses are used to illuminate a pair of photoconductive switches. When the pulse allows conduction across one of the switches, a voltage pulse is launched onto the metallic transmission line addressed by STM. The voltage pulses V_1 and V_2 regulate the voltage between the STM tip and the sample, and modulate (transient) tunnelling current,

$$I(t) = I(V_b) + \frac{dI}{dV}(V_1(t+t_d) + V_2(t)) + \frac{1}{2} \frac{d^2I}{dV^2}(V_1(t+t_d) + V_2(t))^2 + \dots,$$

where V_b denotes the applied DC voltage and t_d denotes the delay time between optical pulses.

When the I - V curve has the nonlinearity $I = \beta(V + \gamma V^3) + O(V^4)$, the tunnelling current induced by the two applied bias voltages provided by a pair of optical pulses can be written as $I(t) = I(V_1(t+t_d) + V_2(t)) \neq I(V_1(t+t_d)) + I(V_2(t))$. Thus, the measured time-resolved tunnelling current is given by

$$I_{tr}(t_d) = \overline{I(t)} = \frac{3\beta\gamma}{T_L} \int_0^\infty [V_1(t+t_d)V_2^2(t) + V_1^2(t+t_d)V_2(t)] dt,$$

where T_L is the repetition period of pulse trains.

In the pioneering work reported by Nunes and Freeman [38], the technique was tested for detecting voltage pulses propagating along a transmission line, and the temporal resolution was several picoseconds. Since the capacitive coupling linearly depends on voltage, this component does not contribute to the time-resolved signal, in contrast with PG-STM. Therefore, the spatial resolution is expected to be comparable to STM, and the best resolution achieved thus far is 1 nm [41].

The time-resolved measurement with STM is seemingly realized. The time-resolved signal I_{tr} , however, reflects the change in tunnelling current owing to the voltage pulse. Therefore, what I_{tr} reflects is not the carrier dynamics beneath the STM tip but the carrier dynamics

around the gate switches. When one scans the tip and records I_{tr} , the obtained time-resolved image does not reflect the variation of carrier dynamics in the probed area but reflects the variation of electronic states, $\beta\gamma$ in dI/dV [41].

2.3 Pulse-excited STM (PX-STM)

The idea of directly exciting a tip-sample junction by optical pulses was realized first by Hamers *et al* [42, 43]. In this pulse-excited STM (PX-STM), a sequence of single pulses illuminates the junction, and the current through the junction is recorded as a function of the pulse repetition period (interval between pulses) (figure 2(d)). They measured carrier relaxation on Si(111)-(7x7) with 10 ns and 1 μ m resolutions. As described later in detail, for a semiconductor sample, tip-induced band bending (TIBB) occurs beneath the STM tip under a certain voltage condition. When a pulse excites the sample, TIBB relaxes as a result of photocarrier redistribution, leading to a change in the surface potential or surface photovoltage (SPV). SPV relaxes as photocarriers decay, accompanied by a change in the displacement current originating from capacitive coupling between the tip and the sample. As a result of the narrow circuit bandwidth, the measured signal is the time-averaged displacement current, which, however, depends on the repetition period. SPV has a saturation tendency when a sufficient number of photocarriers are generated. Therefore, as the pulse repetition period decreases and becomes smaller than the relaxation time for SPV, SPV becomes almost saturated all the time, resulting in a change in the time-averaged displacement current. Thus, the dependence of displacement current on repetition period reflects the relaxation processes of SPV and photocarrier density.

In order to increase sensitivity, Hamers *et al* modulated the optical intensity and detected the synchronized signal by the lock-in technique. However, intensity regulation causes a

thermal expansion and shrinkage of the tip and sample. Since the tunnelling current is sensitive to the tip-sample distance, the thermal effect should seriously interfere with the current [34, 44-46]. To avoid this, they retracted the tip and measured the displacement current instead of the tunnelling current. By adopting this excellent idea, they demonstrated the application of pair-excited STM to probe carrier dynamics. Since displacement current was probed, the spatial resolution was about 1 μm , and the temporal resolution was determined by the repetition period of laser pulses, which is on the order of 10 ns.

2.4 Shaken-pulse-pair-excited STM (SPPX-STM)

The scheme for applying the pump-probe technique directly to a tip-sample junction is called paired-pulse-excited STM (PPX-STM). In PPX-STM, pump and probe pulses are collimated coaxially and illuminate the junction, and the DC current through the junction is measured as a function of delay time (figure 2(d)). The first attempt at PPX-STM was reported by Pfeiffer *et al* [47]. They observed a laser-induced time-resolved current on tantalum and GaAs(110) in UHV. The observed current was independent of the tip-sample distance, indicating that the current does not originate from tunnelling. From the nonlinear dependence of the signal on optical intensity, they concluded that the signal originates from multiphoton photoelectron emission. They demonstrated a temporal resolution of the pulse duration (subpicoseconds).

A high spatial resolution requires the isolation of the time-resolved tunnelling current from unwanted background currents, such as multiphoton photoemission, and more seriously, interference arising from thermal expansion of the tip. The modulation of optical intensity, as used in the optical pump-probed technique, may be useful for detecting an extremely weak time-resolved tunnelling current (~ 100 fA when the STM feedback current is set to be ~ 100 pA).

In the tunnelling regime, however, it results in serious thermal interference [34, 44-46] comparable to the STM feedback current and spoils the measurement.

This major drawback has been overcome by modulating the delay time instead of optical intensity and by using lock-in detection. This idea has been realized recently and named SPPX-STM [26-32]. In SPPX-STM, the optical intensity is nearly unchanged at the modulation frequency, and hence, the thermal interference is markedly suppressed. This new scheme realizes pump-probe-based STM and allows the detection of time-resolved tunnelling current. In the next section, we discuss the principle of SPPX-STM and show how carrier dynamics is probed by tunnelling current.

3. Basis and results of SPPX-STM

3.1 Principle

Figure 3 shows how SPPX-STM works. The surface of the sample beneath the STM tip is illuminated with a sequence of paired laser pulses with a certain delay time t_d , and the tunnelling current I is measured as a function of t_d . The optical pulses give rise to current pulses in the raw tunnelling current I^* , reflecting the excitation and relaxation of the sample. When t_d is sufficiently long, the paired optical pulses with the same intensity independently induce two current pulses with the same height in I^* (figure 3(a)). In contrast, when t_d is short and the second pulse illuminates the sample in the excited state caused by the first pulse, the second current pulse may have a different height, depending on t_d (figures 3(b) and 3(c)). Thereby, the signal I also depends on t_d , because the height difference in the second current pulse changes the time-averaged value of the tunnelling current. Accordingly, the relaxation dynamics of the excited carriers in the target material, namely, the decay of carrier density after the excitation by the first optical pulse, can be probed by STM.

With the modulation of t_d between t_d^1 and t_d^2 , the in-phase component obtained by the lock-in detection of the tunnelling current gives $\Delta I(t_d^1, t_d^2) \equiv I(t_d^1) - I(t_d^2)$. As t_d^2 is set to a value larger than the relaxation time of the probed dynamics, $\Delta I(t_d^1, t_d^2)$ can be approximated as $\Delta I(t_d^1, t_d^2) \equiv I(t_d^1) - I(\infty)$, where $I(\infty)$ is the tunnelling current for a delay time that is sufficiently long for the excited state to be relaxed. Therefore, $\Delta I(t_d^1)$ is obtained through the lock-in detection of I by sweeping t_d^1 .

Similar to a pump-probe technique, SPPX-STM has the temporal resolution of the pulse duration (potentially down to several femtoseconds) and a spatial resolution comparable to that of STM. The mechanism by which dynamical processes triggered by optical irradiation appear in the tunnelling current varies with the material system. In the following, the results and mechanism for semiconductors are discussed.

3.2 Example of signal

An example of the ΔI dependence on delay time measured by SPPX-STM is shown in figure 4(a). The sample used was a low-temperature-grown $\text{GaN}_x\text{As}_{1-x}$ ($x=0.36\%$, grown at 720 K). The band gap energy was estimated to be 1.34 eV (923 nm) from the photoluminescence spectra. A mode-locked Ti:sapphire oscillator provides 140 fs pulses at a repetition rate of 90 MHz. The delay-time-dependent current is clearly seen at a positive bias voltage, as shown in figure 4(a); ΔI approaches zero as delay time increases. The best fit to an exponential function gives a decay constant of 440 ps. At a negative bias voltage, in contrast, ΔI is observed to be almost zero, regardless of delay time.

3.3 Origin of signal

What process appears in the time-resolved signal $\Delta I(t_d)$? The measured signal is clearly the time-resolved tunnelling current, because the time-resolved signal sharply decreases with the tip-sample distance [27, 48]. Since the technique used does not involve any gate switch in the measurement system, the time-dependent conductance at the detection gap, $g_s(t)$ in the equation in 2.1, is constant; thereby, the measured signal does not exhibit the effect of the geometric capacitance between the tip and the sample. This rules out other possibilities that may appear in time-resolved signals of, for example, photoemission and those related to displacement current. The thermal expansion effect of the STM tip also does not contribute to the signal, as expected, because the signal is almost zero at negative bias voltages for the sample shown in figure 4. Therefore, what physical phenomena occurring in the sample are reflected in the time-resolved tunnelling current?

In SPPX-STM on a semiconductor, a nanoscale metal-insulator-semiconductor (MIS) junction is formed by the STM tip, tunnelling gap, and sample (figure 5(a)). When a reverse bias voltage is applied to the junction, TIBB occurs in the surface region owing to the leakage of the electric field into the sample [34, 49, 50]. With pulse excitation, the redistribution of photocarriers reduces the electric field and changes the surface potential, and increases the effective bias voltage applied to the tunnel junction. Consequently, the illumination increases I^* due to the reduction in the potential barrier for tunnelling current.

The excited state subsequently relaxes to the original state through two processes. One is the decay of the photocarriers on the bulk side (bulk-side decay) via recombination, drift and diffusion (figure 5(c)). The other is the decay of the carriers trapped at the surface (surface-side decay) via thermionic emission and recombination. Because of the lack of counterpart carriers near the surface, the surface-side decay constant is larger than the bulk-side decay constant. In probing bulk-side decay in a semiconductor sample, the spatial resolution is affected by the

potential below the STM tip, while surface-side decay enables us to observe the effects of, for example, atomic-scale defects on the recombination processes. Both of these decay processes appear in the SPPX-STM signal [48].

Here, we focus on the faster component reflecting the bulk-side carrier density. The first component, bulk-side decay, is probed through the mechanism of absorption bleaching, which typically occurs in pump-probe measurement. When carriers excited by the first optical pulse remain in the excited state, the absorption of the second optical pulse is suppressed [2]; the number of carriers excited by the second optical pulse decreases, depending on the number of remaining carriers. Thus, the second current pulse induced in I^* decreases and depends on t_d , reflecting the decay of the excited carriers after the first-pulse excitation (b and c in figure 3). Accordingly, $\Delta I(t_d)$ gives a measure of the bulk-side carrier density.

Figure 4(b) shows the result of optical pump-probe reflectivity measured in the same sample. In general, the time evolution of pump-probe reflectivity reflects the decay of photogenerated carriers, and the time constant corresponds to the bulk recombination lifetime. The time constant derived from the exponential fit to data in figure 4(b) is 410 ps, which is near the time constant in $\Delta I(t_d)$, and therefore, $\Delta I(t_d)$ shown in figure 4(a) corresponds to the fast component, that is, the decay of bulk-side carrier density.

3.4 Application

As described above, SPPX-STM allows the study of transient photocarrier dynamics by the same mechanism as the optical pump-probe technique. Taking advantage of atomic-scale structural investigation using STM, SPPX-STM has the potential to probe spatial information on local carrier dynamics.

Here, we show spatially dependent carrier recombination in a semiconductor heterostructure

consisting of materials with different lifetimes, GaAs/Al_{0.5}Ga_{0.5}As/LT-GaAs (figure 6), where LT-GaAs represents low-temperature-grown GaAs. The sample was prepared as follows. A layer (1 μm) was grown at 250 °C by molecular beam epitaxy (MBE) on a barrier layer of AlGaAs (1 μm) grown on an undoped GaAs substrate, which was annealed at 700 °C for 60 s in H₂(5 %)/Ar ambient, and contained high-density defects that act as recombination sites for carriers. Thus, its carrier lifetime is much shorter than that of GaAs. The AlGaAs barrier layer has a band gap larger than the optical excitation energy (1.55 eV). Figure 6(b) shows an STM image of the sample cleaved in ultrahigh vacuum. The interfaces of the three layers are clearly recognized. Figure 6(c) shows the SPPX-STM spectra, $\Delta I(t_d)$, taken at certain points in the GaAs, AlGaAs, and LT-GaAs regions. As expected, the LT-GaAs region exhibits an ultrafast decay component with a time constant of 4.0 ps, while the GaAs region exhibits a time constant of 4.8 ns. These values are consistent with the recombination lifetimes determined by the optical pump-probe reflectivity measurement, 1.5 ps and 2.7 ns for the LT-GaAs and GaAs samples, respectively. The negative sign of the signals, which corresponds to the decrease in I , is in good agreement with the absorption bleaching mechanism. These results support the mechanism proposed above. For AlGaAs, there is no delay-time dependence in $\Delta I(t_d)$, because no photocarrier generation occurs in this area.

Here, we gave an example of an SPPX-STM study on carrier recombination; other carrier dynamics such as drift, diffusion and surface-side decay, which also govern the device operation, can be investigated as well [48], indicating a potential for probing various types of dynamics.

4. Summary

We reviewed a wealth of time-resolved microscopy methods based on ultrafast laser technology. The features and drawbacks of each developed microscopy method were discussed,

particularly from the viewpoint of spatial and temporal resolutions. Then, a new microscopy technique, SPPX-STM, which realizes a high spatiotemporal resolution by combining STM with the pump-probe technique and has the potential for imaging of ultrafast dynamics on a femtosecond timescale with a spatial resolution based on STM, was explained in detail. For semiconductor samples, the time evolution of photocarrier density is reflected in the signal of SPPX-STM, $\Delta I(t_0)$. We showed a carrier recombination process as an example, but other dynamical processes, such as carrier drift and diffusion, can be imaged as well, making SPPX-STM applicable for the analysis of various composite materials in future devices. SPPX-STM is also applicable to systems where a response in tunnelling current has a nonlinear dependence on optical intensity. We hope that this new technique will open a window to the further advancement of future research in nanoscale science and technology.

References

- [1] Shinada T, Okamoto S, Kobayashi T and Ohdomari I 2005 *Nature* **437** 1128
- [2] Othonos A 1998 *J. Appl. Phys.* **83** 1789 and references therein
- [3] Shah J 1999 *Ultrafast Spectroscopy of Semiconductors and Semiconductor Nanostructures* (Berlin: Springer) and references therein
- [4] Hagen A, Steiner M, Raschke M B, Lienau C, Hertel T, Qian H, Meixner A J and Hartschuh A 2005 *Phys. Rev. Lett.* **95** 197401
- [5] Levy J, Nikitin V, Kikkawa J M, Cohen A, Samarth N, Garcia R and Awschalom D D 1996 *Phys. Rev. Lett.* **76** 1948
- [6] Cadby A, Khalil G, Fox A M and Lidzey D G 2008 *J. Appl. Phys.* **103** 093715
- [7] Nechay B A, Siegner U, Morier-Genoud F, Schertel A and Keller U 1999 *Appl. Phys. Lett.* **74** 61
- [8] Schmidt O, Bauer M, Wiemann C, Porath R, Scharfe M, Andreyev O, Schönhense G and Aeschlimann M 2002 *Appl. Phys. B* **74** 223
- [9] Kubo A, Pontius N and Petek H 2007 *Nano Lett.* **7** 470
- [10] Schönhense G 2004 *J. Electron. Spectrosc. Relat. Phenom.* **137-140** 769
- [11] Oelsner A, Krasnyuk A, Nepijko S, Schneider C M and Schönhense G 2005 *J. Electron. Spectrosc. Relat. Phenom.* **144-147** 771
- [12] Bauer M, Wiemann C, Lange J, Bayer D, Rohmer M and Aeschlimann M 2007 *Appl. Phys. A* **88** 473
- [13] Meyer zu Heringdorf F –J, Chelaru L I, Möllenbeck S, Thien D and Horn-von Hoegen M 2007 *Surf. Sci.* **601** 4700
- [14] Rohmer M, Ghaleh F, Aeschlimann M, Bauer M and Hövel H 2007 *Eur. Phys. J. D* **45** 491
- [15] King W E, Campbell G H, Frank A, Reed B, Schmerge J F, Siwick B J, Stuart B C and

- Weber P M 2005 *J. Appl. Phys.* **97** 111101 and references therein
- [16] Barwick B, Park S, Kwon O –H, Baskin J S and Zewail A H 2008 *Science* **322** 1227
- [17] Dömer H and Bostanjoglo O 2003 *Rev. Sci. Instrum.* **74** 4369
- [18] LaGrange T, Armstrong M R, Boyden K, Brown C G, Campbell G H, Colvin J D, DeHope W J, Frank A M, Gibson D J, Hartemann F V, Kim J S, King W E, Pyke B J, Reed B W, Shirk M D, Shuttlesworth R M, Stuart B C, Torralva B R and Browning N D 2006 *Appl. Phys. Lett.* **89** 044105
- [19] Reed B W, Armstrong M R, Browning N D, Campbell G H, Evans J E, LaGrange T and Masiel D J 2009 *Microsc. Microanal.* **15** 272
- [20] Gahlmann A, Park S T and Zewail A H 2008 *Phys. Chem. Chem. Phys.* **10** 2894
- [21] Mamin H J, Birk H, Wimmer P and Rugar D 1994 *J. Appl. Phys.* **75** 161
- [22] Wintterlin J, Trost J, Renisch S, Schuster R, Zambelli T and Ertl G 1997 *Surf. Sci.* **394** 159
- [23] Rost M J, Crama L, Schakel P, van Tol E, van Velzen-Williams G B E M, Overgaww C F, ter Horst G, Dekker H, Okhuijsen B, Seynen M, Vijftigschild A, Han P, Katan A J, Schoots K, Schumm R, van Loo W, Oosterkamp T H and Frenken J W M 2005 *Rev. Sci. Instrum.* **76** 053710
- [24] Petersen L, Schunack M, Schaefer B, Linderoth T R, Rasmussen P B, Sprunger P T, Laegsgaard E, Stensgaard I and Besenbacher F 2001 *Rev. Sci. Instrum.* **72** 1438
- [25] Kemiktarak U, Ndukum T, Schwab K C and Ekinci K L 2007 *Nature* **450** 85
- [26] Takeuchi O, Morita R, Yamashita M and Shigekawa H 2002 *Jpn. J. Appl. Phys.* **41** 4994
- [27] Takeuchi O, Aoyama M, Oshima R, Okada Y, Oigawa H, Sano N, Shigekawa H, Morita R and Yamashita M 2004 *Appl. Phys. Lett.* **85** 3268
- [28] Takeuchi O, Aoyama M and Shigekawa H 2005 *Jpn. J. Appl. Phys.* **44** 5354
- [29] Takeuchi O, Aoyama M, Kondo M, Taninaka A, Terada Y and Shigekawa H 2006 *Jpn. J.*

Appl. Phys. **45** 1926

[30] Terada Y, Aoyama M, Kondo H, Taninaka A, Takeuchi O and Shigekawa H 2007 *Nanotechnology* **18** 044028

[31] Shigekawa H, Yoshida S, Takeuchi O, Aoyama M, Terada Y, Kondo H and Oigawa H 2008 *Thin Solid Films* **516** 2348

[32] Shigekawa H, Takeuchi O, Aoyama M 2005 *Science and Technology of Advanced Materials* **6** 582

[33] Binnig G, Rohrer H, Gerber Ch and Weibel E 1982 *Phys. Rev. Lett.* **49** 57

[34] Grafström S 2002 *J. Appl. Phys.* **91** 1717 and references therein

[35] Weiss S, Ogletree D F, Botkin D, Salmeron M and Chemla D S 1993 *Appl. Phys. Lett.* **63** 2567

[36] Keil U D, Jensen J R and Hvam J M 1998 *Appl. Phys. Lett.* **72** 1644

[37] Botkin D, Glass J, Chemla D S, Ogletree D F, Salmeron M and Weiss S 1996 *Appl. Phys. Lett.* **69** 1321

[38] Groeneveld R H M and van Kempen H 1996 *Appl. Phys. Lett.* **69** 2294

[39] Nunes Jr. G and Freeman M R 1993 *Science* **262** 1029

[40] Steeves G M, Elezzabi A Y and Freeman M R 1997 *Appl. Phys. Lett.* **70** 1909

[41] Khusnatdinov N N, Nagle T J and Nunes Jr. G 2000 *Appl. Phys. Lett.* **77** 4434

[42] Hamers R J and Cahill D G 1990 *Appl. Phys. Lett.* **57** 2031

[43] Hamers RJ and Cahill D G 1991 *J. Vac. Sci. Technol.* **B9** 514

[44] Grafström S, Schuller P, Kowalski J and Nuemann R 1998 *J. Appl. Phys.* **83** 3435

[45] Gerstner V, Knoll A, Pfeiffer W, Thon A and Gerber G 2000 *J. Appl. Phys.* **88** 4851

[46] Jersch J, Demming F, Fedotov I and Dickmann K 1999 *Appl. Phys.* **A68** 637

[47] Pfeiffer W, Sattler F, Vogler S, Gerber G, Grand J. –Y and Möller R 1997 *Appl. Phys.* **B64**

[48] Terada Y, Yoshida S, Aoyama M, Kondo H, Okubo A, Takeuchi O, Oshima R, Okada Y, Yamaguchi H, Hirayama Y and Shigekawa H to be published elsewhere

[49] Yoshida S, Kikuchi J, Takeuchi O, Oigawa H and Shigekawa H 2006 *e-journal, Surf. Sci. Nanotech.* **4** 192

[50] Yoshida S, Kanitani Y, Oshima R, Okada Y, Takeuchi O and Shigekawa H 2007 *Phys. Rev. Lett.* **98** 026802

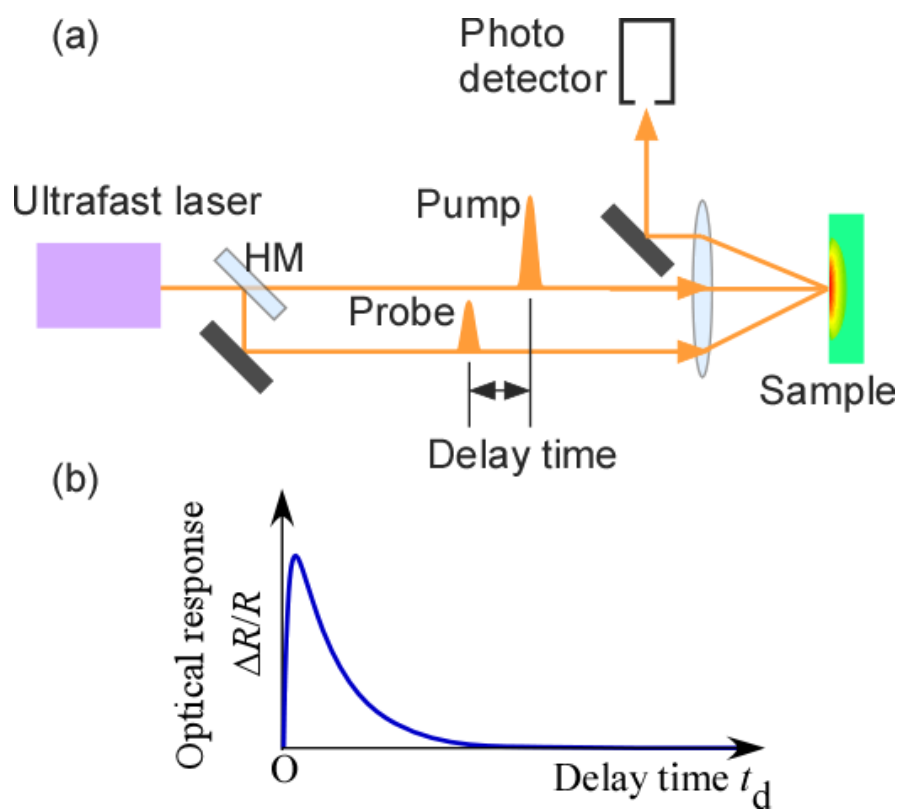


Figure 1 Fundamentals of optical pump-probe technique. (a) Experimental setup of pump-probe reflectivity measurement. HM denotes half-mirror. (b) Typical signal curve showing $\Delta R/R$ vs delay time (R: reflectivity).

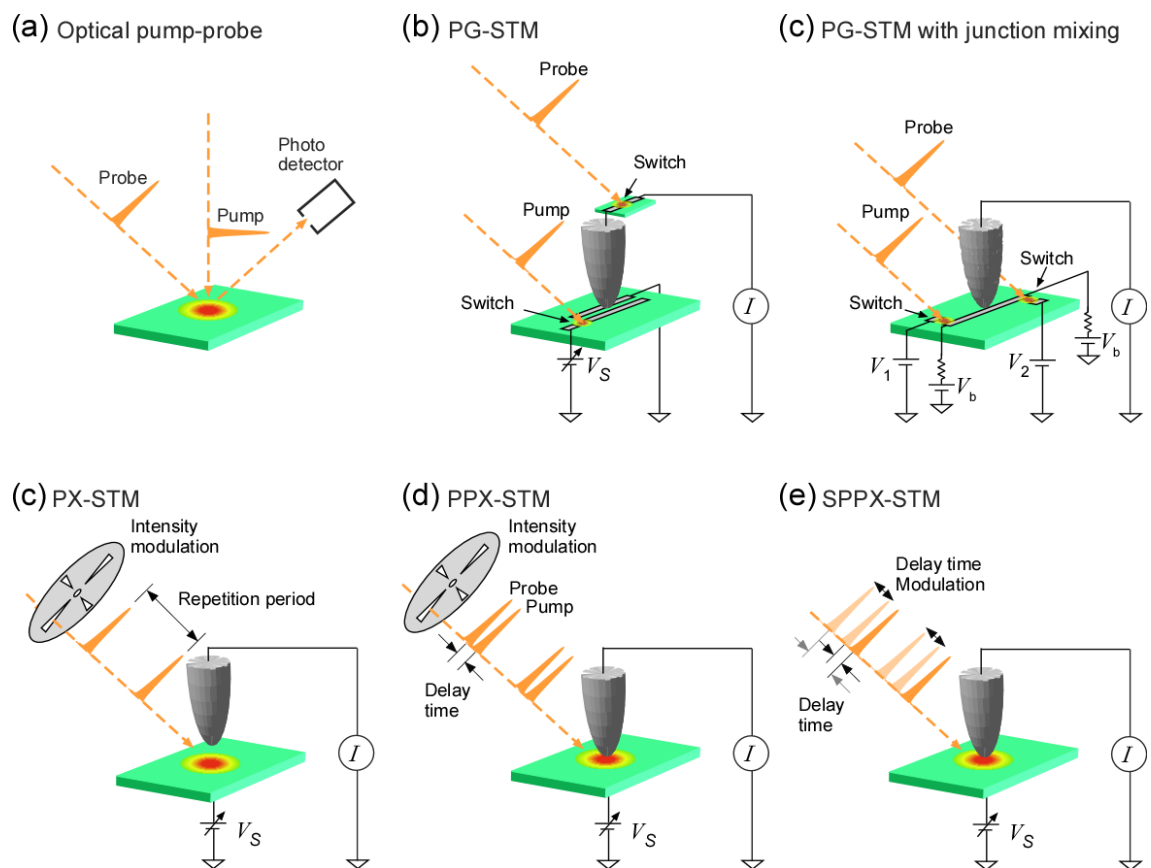


Figure 2 (a) Scheme of optical pump-probe technique. (b)-(e) Various combinations of STM with ultrashort pulse laser technology.

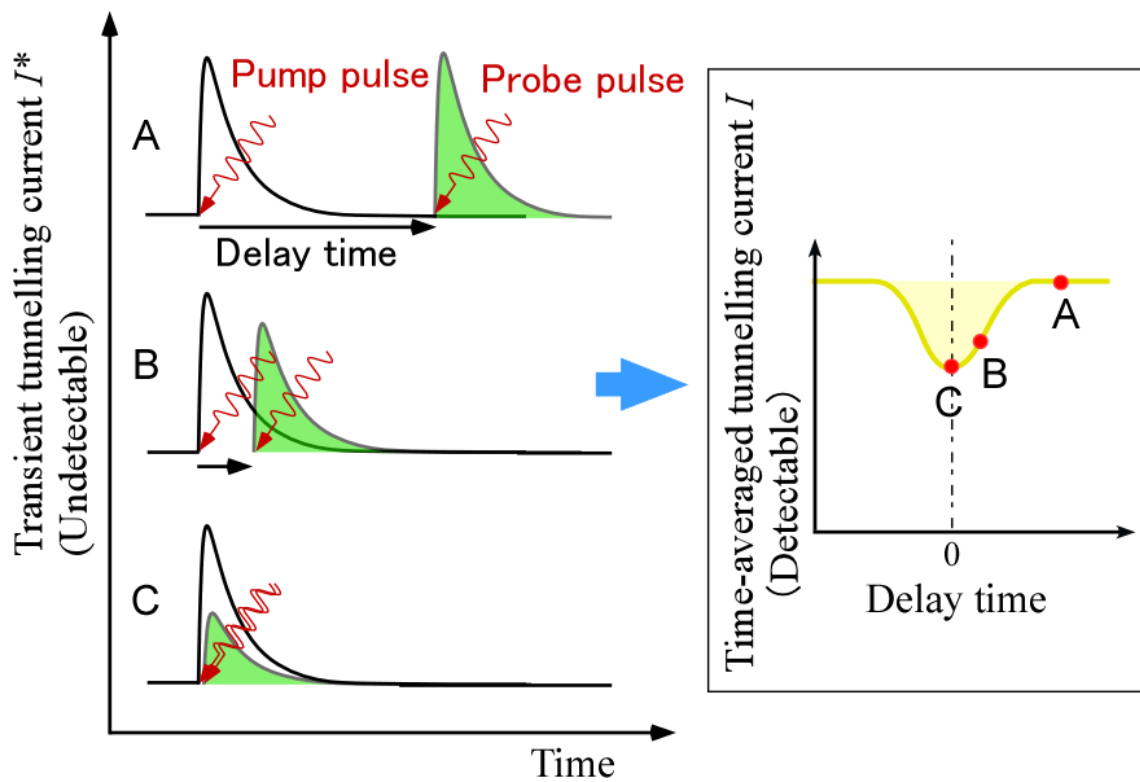


Figure 3 Relationship between delay time and transient tunnelling current I^* (left), and corresponding time-averaged tunnelling current I measured as a function of delay time (right).

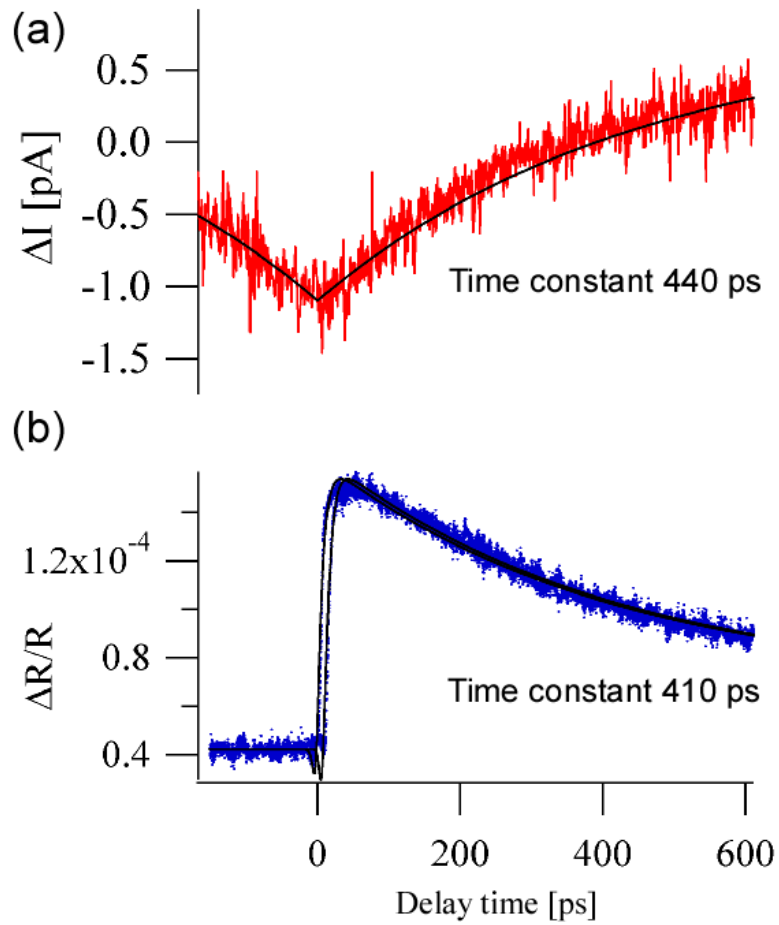


Figure 4 Results for $\text{GaN}_x\text{As}_{1-x}$ ($x=0.36\%$) sample. (a) SPPX signal (red) and exponential fit to data (black). Excitation energy was 1.38 eV (wavelength of 900 nm), averaged intensity was 5 mW, sample bias was 4 V, and feedback current was 200 pA. (b) Delay-time dependence of reflectivity change (blue) measured by optical pump-probe technique, and fit to data (black). Excitation energy was 1.55 eV (wavelength of 800 nm), averaged intensity was 1 mW for pump and 0.1 mW for probe.

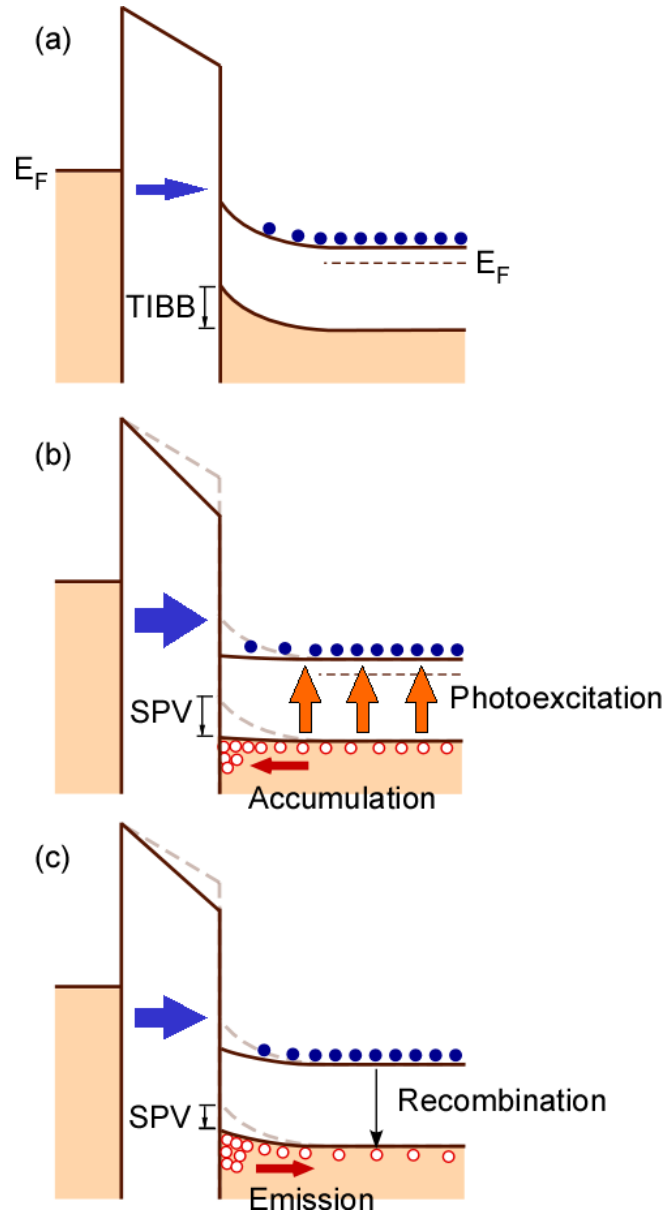


Figure 5 Time evolution of band structure for n-type semiconductor, and optical response in tunnelling current. (a) Before pulse illumination (dark state). (b) Immediately after pulse illumination. (c) During photocarrier relaxation

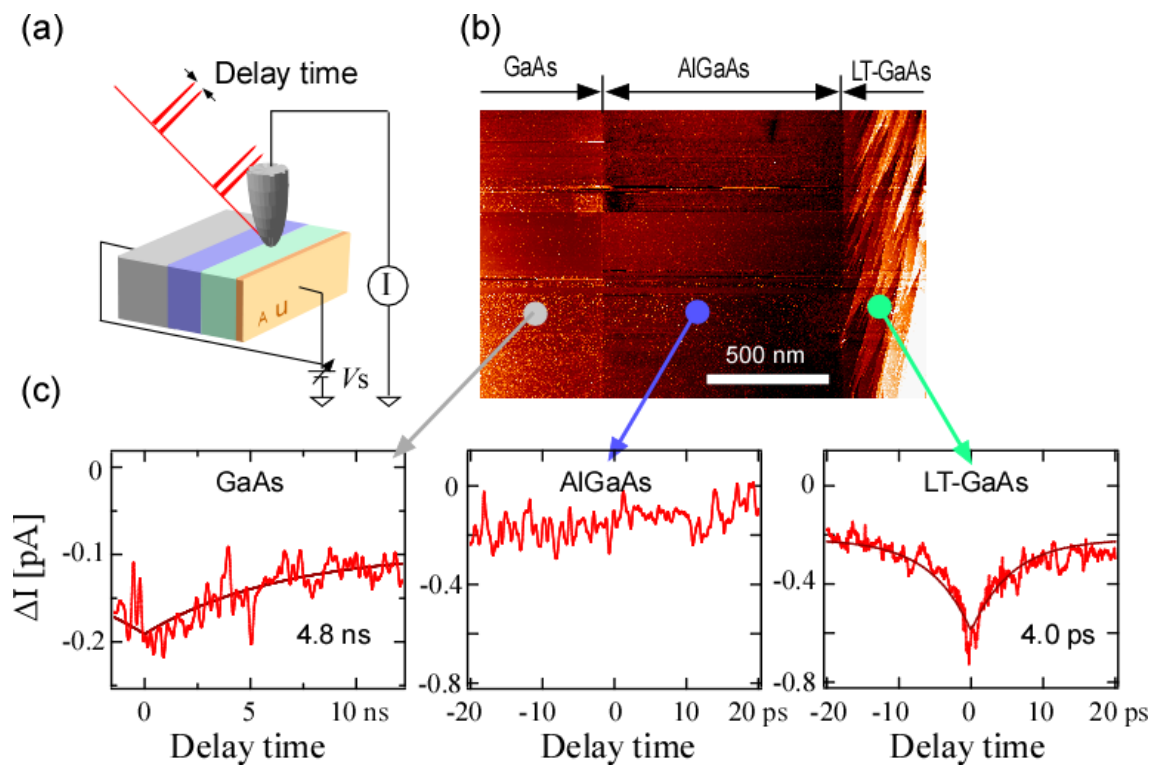


Figure 6 SPPX-STM measurement for GaAs/AlGaAs/LT-GaAs heterostructure. (a) Schematic of measurement. (b) STM image of cleaved surface. (c) SPPX-STM signals observed at each region.